INTERNATIONAL JOURNAL OF HYDROGEN ENERGY 40 (2015) 9335–9346

Available online at www.sciencedirect.com

ScienceDirect

journal homepage: www.elsevier.com/locate/he

Hydrogen storage properties of $LiNH_2$–LiH system with MgH_2, CaH_2 and TiH_2 added

G. Amica, P. Arneodo Larochette, F.C. Gennari*

Centro Atómico Bariloche (CNEA) – Instituto Balseiro (Universidad Nacional de Cuyo), Consejo Nacional de Investigaciones Científicas y Técnicas (CONICET), Av. Bustillo 9500, R8402AGP S.C. de Bariloche, Río Negro, Argentina

ARTICLE INFO

Article history:
Received 13 March 2015
Received in revised form
8 May 2015
Accepted 15 May 2015
Available online 10 June 2015

Keywords:
Lithium amide
Ball milling
Calcium hydride
Magnesium hydride
Kinetics

ABSTRACT

The addition of different metal hydrides to Li–N–H system offers a possible way to modify its thermodynamic properties and/or the dehydrogenation/hydrogenation kinetics. In this paper we report the hydrogen storage properties of $LiNH_2$–LiH system with MH_2 added (M = Mg, Ca, Ti) and clarify the chemical interactions occurring during hydrogen cycling. Detailed structural investigations reveal that during heating under hydrogen, MH_2 (M = Mg, Ca) reacts with $LiNH_2$ to form $Li_2Mg(NH)_2$ and $2CaNH–Ca(NH_2)_2$ solid solution, with simultaneous hydrogen release. Formation of the $Li_2NH–CaNH$ mixture after dehydrogenation of the $LiNH_2$–LiH with CaH_2 added is proved by XRPD and FTIR, providing a new reversible pathway for hydrogen storage in the Li–Ca–N–H system. Notable improvement in the dehydrogenation temperature and kinetics was observed for $LiNH_2$–LiH system with CaH_2 and MgH_2 added, without clear effects in the case of TiH_2. The kinetic analysis reveals that dehydrogenation process is diffusion-controlled and the beneficial effect of MgH_2 and CaH_2 is due to the enhancement of Li^+ mobility.

Introduction

Hydrogen storage remains one of the most challenging technological barriers to the advancement of hydrogen fuel cell technologies for mobile applications. Although there are a variety of ways to store hydrogen, solid-state hydrogen storage provides improved volumetric energy densities in comparison with compressed gas or liquid hydrogen, with a combination of safe and efficient conditions at moderate pressure and temperatures. Recently, much attention has been focused on complex metal hydrides storage systems, such as borohydrides and amides [1–11]. In particular, the lithium amide ($LiNH_2$)-lithium hydride (LiH) system has been proposed as a possible candidate [7], because it offers relatively high gravimetric storage capacity (6.5 wt.% of theoretical value) and reversibility in the hydrogen storage:

$$LiNH_{2(s)} + LiH_{(s)} \leftrightarrow Li_2NH_{(s)} + H_{2(g)} \quad (1)$$

However, the temperatures required for the dehydrogenation/rehydrogenation of reaction (1) are still too high for the application of Li–N–H system as commercial hydrogen

* *Corresponding author*. Instituto Balseiro (UNCuyo), Centro Atómico Bariloche (CNEA) and Consejo Nacional de Investigaciones Científicas y Técnicas (CONICET), Av. Bustillo 9500, R8402AGP S. C. de Bariloche, Argentina. Tel.: +54 294 4445118; fax: +54 294 4445190.
E-mail address: gennari@cab.cnea.gov.ar (F.C. Gennari).
http://dx.doi.org/10.1016/j.ijhydene.2015.05.091

storage material. One strategy to modify the thermodynamic properties with positive effects on the kinetics is the development of new ternary metal–N–H systems, such as Li–Mg–N–H [12–15], Li–Al–N–H [16–18], Li–Ca–N–H [19–22] and others as Li–Ti–N–H [10,23–25], which were investigated on their interaction with hydrogen. In fact, different improvements in the dehydrogenation rates and/or in the thermodynamic parameters were observed by substituting LiH with MgH_2. Luo et al. [12] studied the dehydrogenation of a mixture of $2LiNH_2$–MgH_2 and showed that $LiNH_2$ reacts with MgH_2 to form Li_2NH, MgNH, and H_2 as products, with better hydrogen storage performance than Li–N–H system. The decomposition enthalpy for the $2LiNH_2$–MgH_2 mixture was found to be 34 kJ/mol of H_2, which means a relevant reduction compared to 51 kJ/mol for the $LiNH_2$–LiH mixture [13]. Initially, it was thought that Li_2NH and MgNH constitute the products of dehydrogenation of the $2LiNH_2$–MgH_2 mixture. Additional studies demonstrate that the dehydrogenated sample contain $Li_2Mg(NH)_2$ and the rehydrogenated product obtained from $Li_2Mg(NH)_2$ is not $2LiNH_2 + MgH_2$ but $Mg(NH_2)_2 + 2LiH$ [15], as described in:

$$2\,LiNH_{2(s)} + MgH_{2\,(s)} \rightarrow Li_2Mg(NH)_{2\,(s)} + 2H_{2\,(g)} \leftrightarrow Mg(NH_2)_{2\,(s)} + 2\,LiH_{\,(s)} \quad (2)$$

Xiong et al. [8] and Wu [21] reported that hydrogenation/dehydrogenation behavior and final products of the interaction in Li–Ca–N–H and Li–Mg–N–H systems are comparable. For example, $Li_2Ca(NH)_2$ was synthesized by dehydrogenation of $LiNH_2$–$2CaH_2$, in similar way than $Li_2Mg(NH)_2$ is obtained by the reaction (2). However, dehydrogenation from the $2LiNH_2$–CaH_2 mixture starts at about 70 °C, while for $LiNH_2$–MgH_2 and $LiNH_2$–LiH composites hydrogen release was observed over 100 °C and 150 °C, respectively [8]. Although $2LiNH_2$–CaH_2 mixture (~4.5 wt.%) has lower hydrogen capacity than $LiNH_2$–MgH_2 (~5.5 wt.%), it was demonstrated that the mechanism of the reversibility involves the formation of $CaNH + Li_2NH$ in the hydrogenated state [21]:

$$2\,LiNH_{2(s)} + CaH_{2\,(s)} \rightarrow CaNH_{(s)} + Li_2NH_{(s)} + 2H_{2(g)} \leftrightarrow Ca(NH_2)_{2\,(s)} + 2LiH_{(s)} \quad (3)$$

The appearance of $Li_2Ca(NH)_2$ is only possible after the previous formation of CaNH and Li_2NH during dehydrogenation at high temperature (>300 °C). Further work using different $LiNH_2$–CaH_2 molar ratios (2:1, 3:1 and 4:1) [22] demonstrates that reaction involved in the reversibility depends on the starting molar ratio. In the case of 4:1 molar ratio, the $LiNH_2$–CaH_2 mixture transforms to a new compound with a composition of $Li_4CaN_4H_6$ during dehydrogenation, while rehydrogenation gives $LiNH_2$, LiH and the solid solution $CaNH–Ca(NH_2)_2$ [22]. So far, the hydrogen storage reversibility pathway for Li–Ca–N–H system shows different compounds depending on local composition changes and temperature/pressure conditions [19,20,22].

In the case of Ti metal as possible doping of $LiNH_2$, diverse Ti-containing additives were reported as the effective catalysts in the Li–N–H system [23–25]. Excellent reversibility was shown in the presence of $TiCl_3$, but the hydrogen storage capacity was reduced [23]. In addition, the effect of Ti compounds with different sizes was also examined [24]. The studies revealed that nanoparticles of Ti or TiO_2 were effective in reducing the desorption temperature. However, micron-sized Ti and TiO_2 did not show a good catalytic effect. Therefore, it was suggested that the particle size of the precursor may be an important factor to act as an effective catalyst. Studies using X-ray absorption spectroscopy measurements [26] indicate that the Ti atoms in the Ti compounds have a common electronic state, in particular suggests the formation of $TiCl_3.5NH_3$. Nevertheless, any of these studies includes the use of TiH_2 in enough amounts to form the $LiNH_2$–$2TiH_2$ mixture. A possible reaction between $LiNH_2$–$2TiH_2$ involves the formation of Ti_2N and LiH as solid products during dehydrogenation [27]. Using density functional theory calculations, the enthalpy of this reaction was estimated to be low, but this needs to be investigated experimentally.

Motivated by these previous investigations, a comparative study of the hydrogen storage properties of $LiNH_2$–LiH system with MH_2 added (M = Mg, Ca and Ti) was performed using constant amount of additive and same experimental conditions. In this work, different interactions between MH_2 and $LiNH_2$ were identified, which determine the nature of the reversible reaction. The analysis was extended in order to examine the effect of additive on the thermodynamics and kinetics of the Li–N–H system. A proposal of the reaction pathway for each system is further discussed.

Experimental

Synthesis of the composites

The starting materials were commercial $LiNH_2$ (Aldrich, 95%), LiH (Fluka, 95%), TiH_2 (Aldrich, 98%), CaH_2 (Merck, 95%) and MgH_2 (Aldrich, 98%), which are referred as LN, L, Ti, Ca and Mg, respectively. All samples were handled in an MBraun Unilab glove argon-filled glove box, with oxygen and moisture levels lower than 1 ppm. For all studies, high purity hydrogen (Linde, 99.999%) and argon (Linde, 99.999%) were used.

The sample preparation was carried out by mechanical milling of the following mixtures: $LiNH_2$-1.6LiH (LNL), $LiNH_2$-1.6LiH-0.2TiH_2 (LNLTi), $LiNH_2$-1.6LiH-0.2CaH_2 (LNLCa) and $LiNH_2$-1.6LiH-0.2MgH_2 (LNLMg). The amount of LiH was added in excess to minimize the emission of NH_3 [18]. The mechanical milling was performed using a sequence of 15 min milling and 10 min pause in a planetary ball mill at 500 rpm (Fritsch Pulverisette 6) under 0.1 MPa of argon. About 1.5 g of mixture was placed in an 80 mL stainless steel mill chamber with 5 stainless steel balls of 14.5 mm of diameter. To avoid NH_3 emission, the mill chamber was opened after 1 h, 2 h and 3 h to mix the powders and eliminate possible dead zones. All samples were ball milled for 5 h with a ball to powder ratio of 53:1.

Characterization of the composites

Structural, textural, thermal and hydrogen storage properties of the as-milled and as-cycled samples were studied using differential scanning calorimetry (DSC, TA 2910 calorimeter), powder X-ray diffraction (XRPD, Philips PW 1710/01

Instruments), Fourier transform infrared spectroscopy (FTIR, Perkin Elmer Spectrum 400), thermogravimetry (TG-HP50, TA Instruments) and Sieverts-type volumetric equipment.

Structural information of the samples was obtained by XRPD (Cu Kα radiation, graphite monochromator) and FTIR analyses. During the XRPD data collection all the samples were maintained under Ar atmosphere using a tightly sealed sample holder to prevent the reaction between samples and air. For IR spectroscopy measurements, the samples were grounded with dry KBr under purified argon atmosphere and pressed to pellets. Solid state IR spectra were obtained in the range of 4000–800 cm^{-1} using a specially designed cell. During dehydrogenation, the gases released were collected in a degassed quartz optical cell with KBr windows and the gas phase spectra were taken at room temperature. No NH_3 emission was detected by gas-FTIR analysis during sample decomposition.

The thermal behavior of the samples was studied by DSC using heating ramps between 1 and 10 °C/min and argon flow rate of 122 ml min^{-1}. About 3–5 mg of sample was loaded into aluminum capsules closed in a glove box. The values obtained were compared with that of the additive free sample. Kissinger's method was employed to determine the activation energy (E_a) and the pre-exponential factor (A):

$$\ln\left(\frac{\beta}{T_m{}^2}\right) = \ln\left(\frac{A\cdot R}{E_a}\right) - \frac{E_a}{R\cdot T_m} \quad (4)$$

where T_m is the peak temperature at which the maximum reaction rate is attained, β is the heating rate and R is the gas constant. The activation energy estimation neglects the formation of minor amounts of NH_3, which could be undetected by FTIR.

The weight change of hydrogenated samples was measured using a 5 °C/min of heating rate and helium gas flow. Samples of about 7–10 mg were loaded into the same type of aluminum capsules than that used for DSC measurements. The capsules were closed in a glove box to minimize the reaction with air during sample transfer.

Pressure-composition isotherms (PCI) and hydrogen sorption kinetics were obtained using modified Sieverts-type equipment, coupled with a mass flow controller. The sample was transferred in the glove box into a stainless reactor which was connected to the Sieverts device. For isothermal measurements, each sample was heated up to the reaction temperature (300 °C) under hydrogen pressure (0.7 MPa) and kept at this temperature for 30 min before measuring the hydrogen desorption/absorption reaction Dehydrogenation curves were obtained at 300 °C under vacuum (0.01 MPa). The rehydrogenation curves were measured at 300 °C at a constant hydrogen pressure of 0.7 MPa. The amount of absorbed/desorbed hydrogen was determined with a relative error <5%. For non-isothermal measurements, the sample was heated at ~5 °C/min from room temperature up to 300 °C at 0.7 MPa of hydrogen pressure. To perform PCI measurements each sample was heated up to 300 °C under 1.5 MPa of hydrogen pressure for 0.5 h before to measure the dehydrogenation PCI curve. The hydrogen contents reported in this paper are expressed as wt.% with respect to the total mass of each mixture. The conversion α was calculated for dehydrogenation curves as the hydrogen released at each time wt.% (t) with respect to the final hydrogen storage.

Results and discussion

Dehydrogenation/hydrogenaton properties of LNLX (X = Mg, Ca, Ti)

The hydrogen desorption performance of the as-milled LNLX samples was evaluated by TG and DSC. The results are displayed in Fig. 1A and B. For comparison, TG and DSC curves of the pristine LNL are also included. TG measurements revealed that the dehydrogenation temperature of LNL (160 °C) was lowered 15 °C by the addition of MgH_2 and CaH_2 (estimated at 0.15% of mass change, Fig. 1A). No modification in the hydrogen release temperature of pristine material was observed by TiH_2 addition. In fact, dehydrogenation rates for LNL and LNLTi samples are similar, considering the molar mass of TiH_2 added. Interestingly, hydrogen release from LNLMg and LNLCa practically finished at 300 °C as a consequence of improved hydrogen desorption rate. In opposition, both LNL and LNLTi samples continue releasing hydrogen up to 400 °C. In agreement with this observation, the shapes of DSC curves for LNL and LNLTi (Fig. 1B) were different from the others, which consist of a main peak and a shoulder peak that end at 400 °C. Moreover, the DSC curves for LNLMg and LNLCa have similar shape, with the main endothermic peak finishing before 300 °C. At this point it is important to remark that the maximum of the endothermic peak associated with the $LiNH_2$ decomposition appears at low temperature for LNLCa (234 °C) respect to LNLMg (244 °C). This shift between TG and DSC measurements for LNLMg seems to be associated with the occurrence of simultaneous reactions (endothermic and exothermic), which will be discussed in the next section.

Table 1 summarizes the mass change in percent calculated from TG curves at 300 °C and 400 °C as well as the theoretical hydrogen storage properties for each composite, assuming that the main reaction is represented by (1). There is a good correlation between theoretical and experimental values for all composites, except for LNLMg system. In this case, 5.6% of mass change was measured in comparison with 5.0 wt.% of theoretical hydrogen storage, suggesting the formation of other gaseous species than hydrogen (see next section).

To evaluate the influence of each additive on the hydrogen sorption behavior, isothermal measurements were carried out at different temperatures. Fig. 2A shows dehydrogenation curves obtained for LNLX samples at 300 °C and 0.02 MPa of hydrogen. Hydrogen release rates evidence the beneficial effect of the CaH_2 and MgH_2 as additives. In fact, dehydrogenation rate for LNLMg and LNLCa is at least two and three times higher than that with respect to that of pristine LNL sample. For LNLTi sample, no favorable influence was observed. Regarding the hydrogen storage capacities, Table 1 summarizes the values obtained after isothermal dehydrogenation (Fig. 2A) with those determined from TG measurements (Fig. 1A). As an interesting detail, the hydrogen storage capacities for LNLMg and LNLCa obtained from volumetric measurement (2.8 and 3.8 wt.%, respectively) are very different from that calculated using TG curves up to 300 °C (5.4 and 4.7 wt.%) and lower than those corresponding to LNL and LNLTi samples. This point will be clarified in the next section.

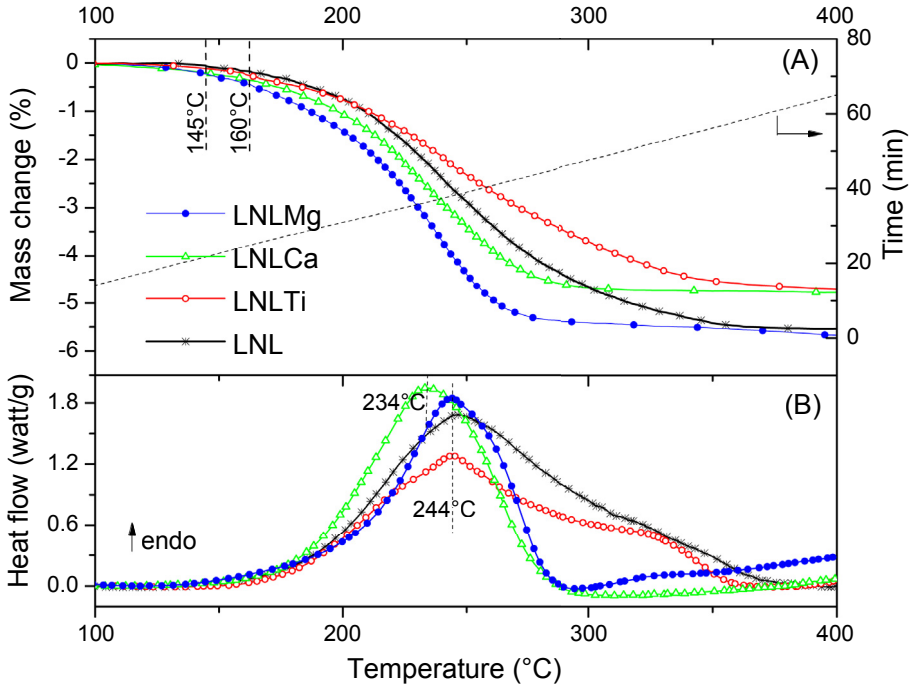

Fig. 1 – TG (A) and DSC (B) curves of the LNL and LNLX samples (X = Mg, Ca and Ti).

Table 1 – Theoretical hydrogen storage compared with the mass change (%) and hydrogen released (wt.%) determined from TG and volumetric measurements, respectively.

Sample	Theoretical hydrogen storage[a]	TG (mass change %)		Isothermal dehydrogenation (wt.%)
		300 °C	400 °C	300 °C
LNLMg	5.0	5.4	5.6	2.8
LNLCa	4.5	4.7	4.7	3.8
LNLTi	4.4	4.0	4.6	4.2
LNL	5.6	4.9	5.5	4.3

[a] Determined on the basis of reaction (1).

For comparative purpose, the kinetic behavior of the samples with MH_2 added was analyzed after some consecutive cycles of dehydrogenation and rehydrogenation (Fig. 3). As general behavior, a reduction in both the hydrogen storage capacity and dehydrogenation rate was observed for each sample with hydrogen cycling. The LNLCa is the best composite in relation with the dehydrogenation rate and the reversible hydrogen storage capacity (about 3.8 wt.%), which is released in 17 min. Although this composite displays the faster dehydrogenation rate, it decreases from the cycle 1 to 8 by a factor of 2 at least.

Structural changes of LNLX (X = Mg, Ca, Ti) after ball milling and dehydrogenation/hydrogenation cycles

Fig. 4 shows the XRPD patterns and FTIR spectra of pristine and samples with MH_2 added after ball milling for 5 h. From Fig. 4A, the phases MgH_2, CaH_2 and TiH_2 are clearly detected after milling of each composite with MH_2 added. The most intense diffraction peaks from LiH are also identified. In addition, all samples exhibited the presence of $LiNH_2$ characterized by the N–H vibrations at 3313 and 3259 cm^{-1} (Fig. 4B). In the case of LNL, the simultaneous presence of Li_2NH is unequivocally demonstrated by the identification of the band at 3180 cm^{-1}. No modification in the N–H vibration energy is indicative that there was not reaction between $LiNH_2$ and MH_2 during the milling process. Moreover, the characteristic band of LiOH (3677 cm^{-1}) was detected in some cases, possibly due to the contact of the pellet with moisture during FTIR cell-handling (wave number region not shown). Then, the mechanical milling for 5 h provides a physical mixture of the starting materials.

To understand the differences observed during dehydrogenation/hydrogenation behavior of the samples with MH_2 added, their structural characteristics after hydrogen cycling were studied. Fig. 5 shows the XRPD patterns and FTIR spectra of LNL and LNLX hydrogenated samples obtained after successive dehydrogenation/hydrogenation cycles at 300 °C (about 5 cycles). As illustrated in Fig. 5A, characteristic diffraction peaks of the starting $LiNH_2$ and LiH are still detected for all samples. In fact, no new phases were detected by XRPD for LNL and LNLTi after cycling, other than the starting materials. However, relevant structural changes were clearly identified for LNLMg and LNLCa composites. Interestingly, the most intense diffraction peaks and the FTIR band at 3176 cm^{-1} associated with $Li_2Mg(NH)_2$ were observed for the LNLMg sample as a consequence of hydrogen cycling. In addition, XRPD pattern of LNLCa also shows modifications in comparison with as-cycled LNL,

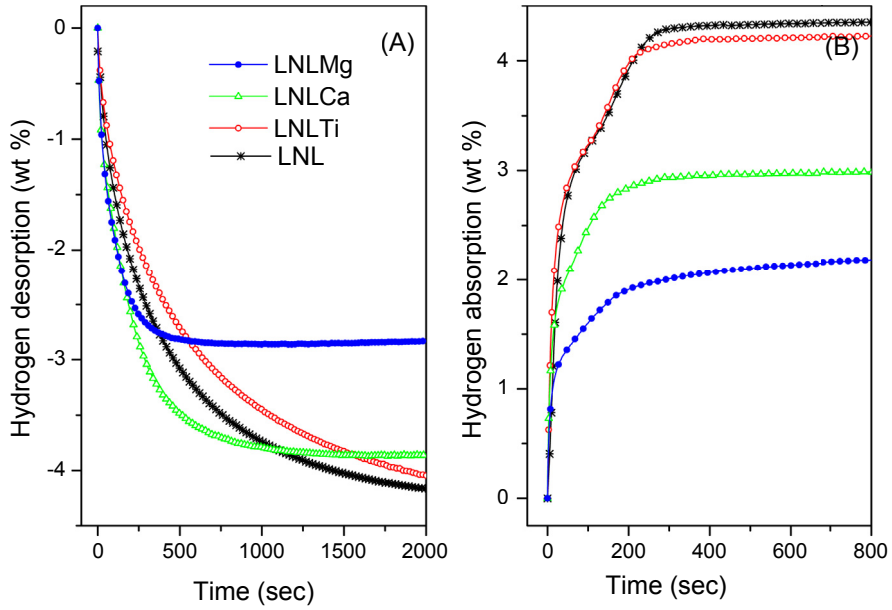

Fig. 2 – Isothermal dehydrogenation (A) and rehydrogenation (B) curves at 300 °C of the LNL and LNLX samples (X = Mg, Ca and Ti). Absorption hydrogen pressure: 0.7 MPa; Desorption hydrogen pressure: 0.02 MPa.

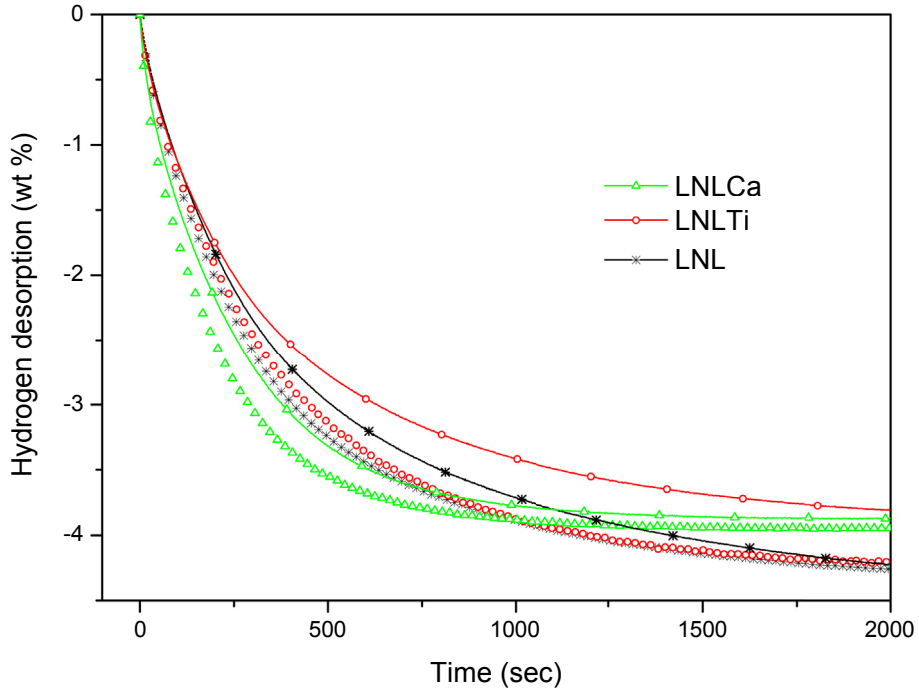

Fig. 3 – Isothermal dehydrogenation at 300 °C of the LNL and LNLX samples (X = Ca and Ti). Desorption hydrogen pressure: 0.02 MPa. Symbols: cycle 3. Straight line with spaced symbols: cycle 8.

in particular the strong intensity of the peaks at $2\theta = 35.3°$ and 50.7°. According to previous published results [22,28], these peaks were associated with the formation of a solid solution $2CaNH{-}Ca(NH_2)_2$. The FTIR bands at 3227 cm^{-1} and 3148 cm^{-1}, previously related with the solid solution $2CaNH{-}Ca(NH_2)_2$, confirms its formation under cycling simultaneously with the presence of extra amount of $LiNH_2$ (bands at 3313 cm^{-1} and 3259 cm^{-1}).

From the above results, it is clear that CaH_2 and MgH_2 interact in different ways with $LiNH_2$-1.6LiH influencing their hydrogen storage properties. However, this interaction could be occur during thermal treatment under hydrogen (0.7 MPa

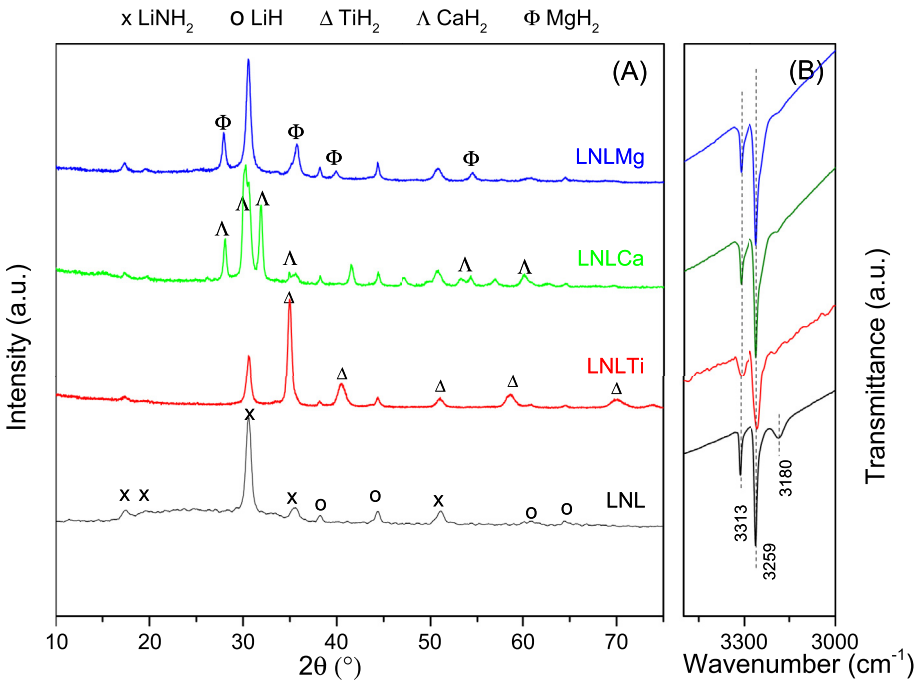

Fig. 4 – XRPD patterns (A) and FTIR spectra (B) of the as-milled LNL and LNLX samples (X = Mg, Ca and Ti).

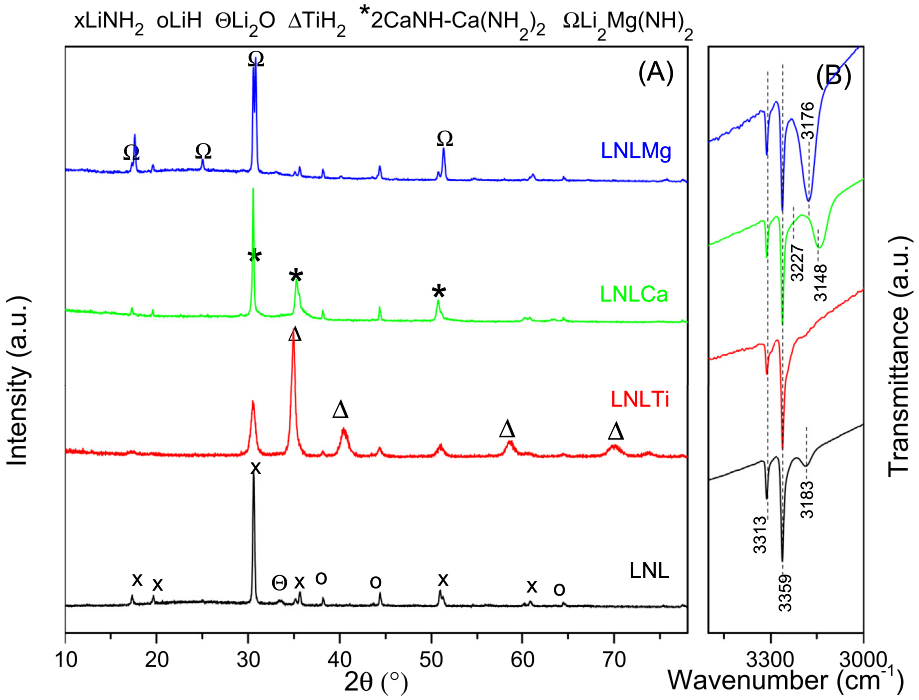

Fig. 5 – XRPD patterns (A) and FTIR spectra (B) of hydrogenated LNL and LNLX samples (X = Mg, Ca and Ti) after cycling.

for 0.5 h at 300 °C) performed before the first dehydrogenation stage. Supporting this idea, relevant differences in the hydrogen storage capacities were obtained from TG and isothermal dehydrogenation (Table 1). Combination of volumetric measurements with XRPD/FTIR studies help to elucidate the reactions between the materials during heating under hydrogen. Fig. 6 shows hydrogenation curves achieved during heating up to 300 °C under 0.7 MPa of hydrogen (heating ramp ~5 °C/min). For comparison, the curve corresponding of LNL is also shown. During heating under pressure, apparent slight hydrogen absorption for LNL and LNLCa samples is observed. In opposition, for LNLMg sample, no

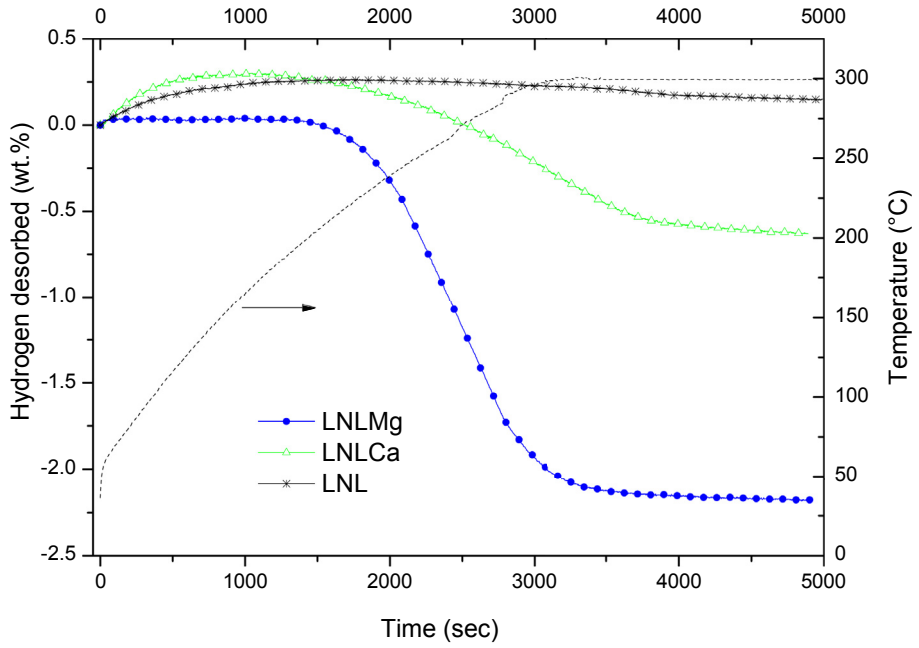

Fig. 6 – Heating up to 300 °C of the LNL and LNLX samples (X = Mg, Ca) under 0.7 MPa of hydrogen.

clear interaction with hydrogen was measured up to 200 °C. After additional heating up to 300 °C, LNLMg and LNLCa systems release 2.2 wt% and 0.6 wt% of hydrogen, as evidence of the interaction between reactants (see Fig. 6). To clarify the nature of the reactions, these samples were studied after heating by combination of FTIR and XRPD techniques (Fig. 7A and B, respectively). From Fig. 7A, the cubic phase of $Li_2Mg(NH_2)_2$ is clearly identified in the LNLMg, simultaneously with $LiNH_2$ and LiH phases. The most intense peaks associated with MgH_2 are absent. It is also seen from this pattern that there are weak unknown peaks at 2θ positions of 12.4, 21.6, 25.0, 33.3 and 42.0°. In the FTIR spectrum for LNLMg, in

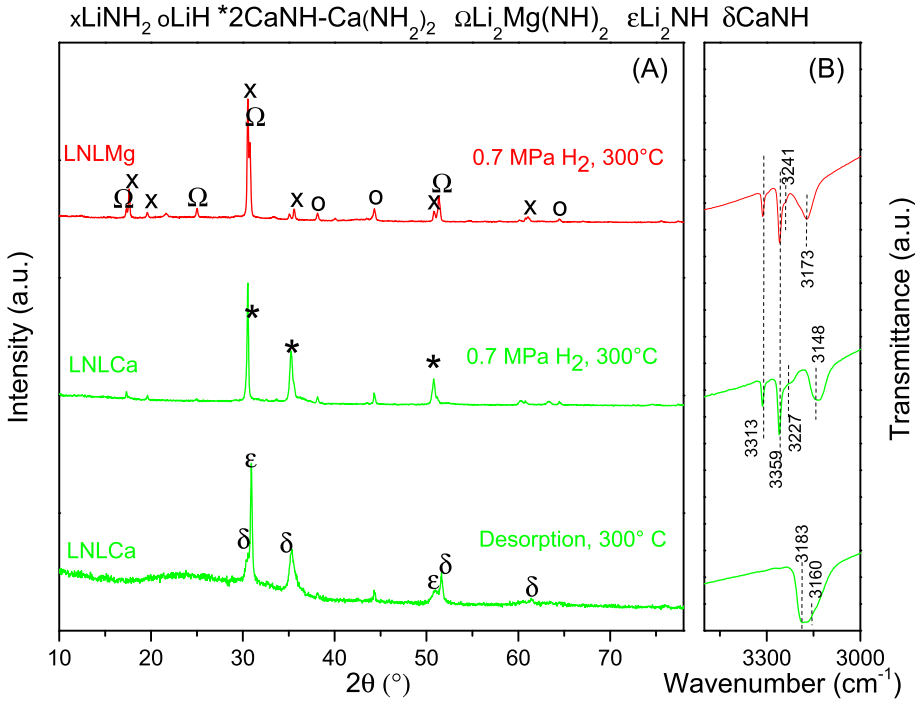

Fig. 7 – XRPD patterns (A) and FTIR spectra (B) of the LNLX samples (X = Mg, Ca) after heating up to 300 °C under 0.7 MPa of hydrogen. For LNLCa, dehydrogenated state at 300 °C after cycling.

addition to the typical bands of cubic $Li_2Mg(NH_2)_2$ (3173 cm^{-1}) and $LiNH_2$ (3313 cm^{-1} and 3259 cm^{-1}), a weak peak centered at 3241 cm^{-1} is also detected. According to a recent work [29], both the XRPD peaks and FTIR band can be linked with decomposed products owing to the partial decomposition of $Li_2Mg(NH_2)_2$. Then, the reactions that occur during heating under hydrogen can be expressed as:

$$2\ LiNH_{2(s)} + MgH_{2\ (s)} \leftrightarrow Mg(NH_2)_{2\ (s)} + 2\ LiH_{\ (s)} \quad (2a)$$

$$Mg(NH_2)_{2\ (s)} + 2\ LiH_{\ (s)} \leftrightarrow Li_2Mg(NH)_{2\ (s)} + 2H_{2\ (g)} \quad (2b)$$

The formation of $Mg(NH_2)_2$ is a solid–solid exothermic reaction, promoted by intimate contact between the reactants due to milling. Indeed, close scrutiny of *in-situ* XRPD patterns of the $2LiNH_2$–MgH_2 mixture revealed its conversion to $Mg(NH_2)_2$–LiH before dehydrogenation takes place [15]. In our case, this reaction seems to occur during the initial heating and it is followed by $Mg(NH_2)_2$ decomposition to form $Li_2Mg(NH)_2$. Mass loss in TG measurement for LNLMg (Fig. 1A) is observed when reaction (2b) starts, while DSC curve contains information from both exothermic (2a) and endothemic (2b) reactions.

The amount of theoretical hydrogen released if all MgH_2 added reacted with $LiNH_2$ according to reaction (2a and 2b) would be about 2.0 wt.% (see Table 2). Considering that from TG the mass change observed is slightly higher (2.2 wt.%), this result confirms that reaction (2b) and the partial decomposition of $Li_2Mg(NH)_2$ arise. The comparison between the XRPD patterns obtained for LNLMg after cycling and after thermal treatment under hydrogen evidences that the peaks associated with decomposition products disappear as a consequence of hydrogen cycling. This is also confirmed by the absence of the band at 3241 cm^{-1} (Fig. 5B). Then, the extra mass change measured in TG analysis for LNLMg compared with theoretical hydrogen storage (Table 1) is due to the partial decomposition of $Li_2Mg(NH)_2$ to other unknown products, as it was suggested by Ref. [29]. Reversibility of reaction (2b) is possible and $Mg(NH_2)_2$ could be rehydrided [13–15]. However, higher hydrogen pressures than that used in the present study (0.7 MPa) are necessary to form $Mg(NH_2)_2$ from $Li_2Mg(NH)_2$ (Figs. 2 and 3). For this reason, the hydrogen storage capacity of LNLMg sample during heating (Fig. 1) is about 5.3 wt.% (Table 1), while after hydrogen cycling was reduced to about 2.5 wt.%. This fact is due to the lost of 2.0 wt.% of hydrogen released irreversibly (reaction 2a) plus about 0.2 wt.% from $Li_2Mg(NH)_2$ decomposition (Table 2).

The reactivity of LNLCa during heating is different. In the XRPD pattern of LNLCa after heating up to 300 °C under 0.7 MPa, $LiNH_2$ and LiH phases can be identified while CaH_2 disappeared (Fig. 7A). In addition, similar than after hydrogen cycling (Fig. 5A), characteristic peaks of the solid solution 2CaNH–$Ca(NH_2)_2$ were identified. As additional support of solid solution formation, its typical bands at 3227 cm^{-1} and 3148 cm^{-1} are present, simultaneously with those corresponding with $LiNH_2$. Taking into account that during heating under hydrogen both solid solution formation and hydrogen release occur, it can be proposed that the following reaction takes place:

$$4\ LiNH_{2(s)} + 3\ CaH_{2\ (s)} \rightarrow [2CaNH{-}Ca(NH_2)_2]_{\ (s)} + 4LiH_{(s)} + 2H_{2\ (g)} \quad (5)$$

According to reaction (5), if all CaH_2 (0.2 mol) reacts with $LiNH_2$, 0.6 wt.% of hydrogen is evolved (see Table 2). This value is in complete agreement with that measured during heating under 0.7 MPa of hydrogen (Fig. 6, Table 2). As a relevant difference with LNLMg sample, the LNLCa sample displays high hydrogen storage reversibility during cycling (Figs. 2 and 3). XRPD and FTIR studies of the dehydrogenated LNLCa after cycling show the most intense diffraction peaks of Li_2NH and CaNH phases as well as their typical bands at 3160 cm^{-1} and 3183 cm^{-1}, respectively. Therefore, hydrogen storage reversibility of the 2CaNH–$Ca(NH_2)_2$ solid solution involves Li_2NH and CaNH formation in the dehydrogenated state using the un-reacted $LiNH_2$:

$$2\ LiNH_{2\ (s)} + 4\ LiH_{\ (s)} + [2CaNH{-}Ca(NH_2)_2]_{\ (s)} \leftrightarrow 3\ Li_2NH_{\ (s)} + 3\ CaNH_{\ (s)} + 4H_{2\ (g)} \quad (6)$$

Table 2 – Theoretical hydrogen storage calculated from reactions (1), (2b), (5) and (6) and experimental hydrogen released (wt.%) during isothermal volumetric measurements.

Sample	Theoretical hydrogen storage[a]	Theoretical hydrogen storage (first heating under hydrogen)		Theoretical hydrogen storage (during cycling)	Experimental hydrogen storage
		Reaction $LiNH_2 + MH_2$	Reaction $LiNH_2 + LiH$		First dehydrogenation
LNLMg	5.0	2.0[b]	3.0[c]	3.0[c]	2.8
LNLCa	4.5	0.6[b] (1.2)[d]	3.9[c] (2.7)[e]	1.2[d] + 2.7[c]	3.8
LNLTi	4.4	–	4.4	4.4[a]	4.2
LNL	5.6	–	5.6	5.6[a]	4.3

[a] Determined on the basis of reaction (1).
[b] Determined on the basis of reaction (2b) or (5), assuming that all MH_2 added (M = Mg, Ca) reacts with $LiNH_2$.
[c] Determined on the basis of reaction (1) using the un-reacted amount of $LiNH_2$ after reaction (2b) or (5).
[d] Determined on the basis of reaction (6).
[e] Determined on the basis of the reaction (1) using the un-reacted amount of $LiNH_2$ after reaction (5) and (6).

The rehydrogenation of the LNLCa system is possible *via* the occurrence of reaction (6) plus the reversibility of unreacted $LiNH_2$ by reaction (1). According to theoretical calculations (see Table 2), 1.2 wt.% of hydrogen is evolved due to the reaction between $2CaNH{-}Ca(NH_2)_2$ and $LiNH_2$ (reaction 6). The remnant amount of $LiNH_2$ is able to store 2.7 wt.% of hydrogen according to reaction (1) (see Table 2). Therefore, the theoretical storage capacity by combination of reactions (6) and (1) is 3.9 wt.%. This value is in good agreement with the hydrogen storage observed in the first cycle, i.e. 3.8 wt.%. The elucidation of the chemical interactions between $LiNH_2$ and CaH_2 during hydrogen cycling constitutes a novel contribution to the knowledge of the Li–Ca–N–H system.

Kinetic and thermodynamic studies on LNLX (X = Mg, Ca, Ti)

To complete the study of the $LiNH_2$–LiH system with MH_2 added (M = Mg, Ca and Ti), pressure-composition-isotherms (PCIs) of dehydrogenation and rehydrogenation at 300 °C were performed for as-milled LNLX samples (Fig. 8A and B, respectively). Dehydrogenation isotherm for LNL displays an initial plateau up to ~1.4 wt.% at about 0.28 MPa (0.30 MPa) of hydrogen pressure. The PCI displays a slope down toward the complete dehydrogenation. This behavior in the PCI curve of the $LiNH_2$–LiH system can be interpreted on the basis of recent investigations [30,31]. These studies have demonstrated that the $LiNH_2$ and Li_2NH are the dominant phases in the hydrogenated and dehydrogenated states respectively, and different phases with intermediate stoichiometry exist between both compounds. In this context, David et al. [30] proposed a Frenkel defect model based on the migration of Li^+ and H^+ ions for dehydrogenation (and hydrogenation). The recent work of Makepeace et al. [31] demonstrates the formation and evolution of non-stoichiometric intermediate species of the form $Li_{1+x}NH_{2-x}$. Then, the sloping behavior of the PCI curve can be related with the conversion of $LiNH_2$ into Li_2NH, involving the formation of non-stoichiometric species.

The PCI curves for LNLCa and LNLTi show similar shape and behavior that LNL material, with minor changes in the width of the initial plateau and in the equilibrium hydrogen pressure at each amount of hydrogen storage. The variation observed for LNLCa sample seems more evident, where the equilibrium pressure for both the dehydrogenation/hydrogenation process was inferior (0.24 MPa/0.28 MPa) to that for LNL sample (0.28 MPa/0.3 MPa). Probably, the presence of the $2CaNH{-}Ca(NH_2)_2$ solid solution in the LNLCa composite plays a minor influence. However, these changes observed are not enough to confirm a modification in the thermodynamic stability of the system. On the contrary, the addition of MgH_2 significantly increases the equilibrium pressure value respect to the $LiNH_2$–LiH system.

During dehydrogenation of LNLMg, two sloping plateaus are observed: the first at 1.24 MPa and the second plateau at 0.45 MPa. Considering the reactions proposed for LNLMg system (Section 3.2), the first plateau can be associated to decomposition of residual amount of $Mg(NH_2)_2$ (formed during heating with 1.5 MPa) and the second one is related with the decomposition of $LiNH_2$ modified with MgH_2. It is important to mention that the first plateau is not observed in rehydrogenation PCI because the hydrogen pressure is not enough to rehydrogenate $Li_2Mg(NH)_2$. From a thermodynamic point of view, the addition of MgH_2 clearly influences the thermodynamics of the LNL system, in agreement with previous works [12–14], while the addition of CaH_2 and TiH_2 has a marginal effect.

Furthermore, dehydrogenation activation energies of the as-milled LNLX samples were calculated by Kissinger's method and the values obtained were compared with that of

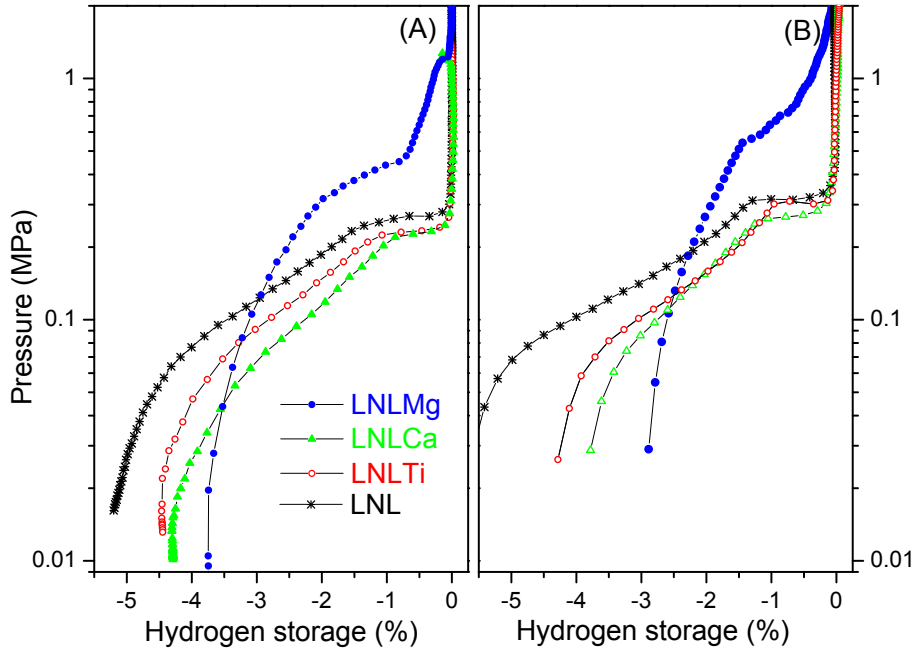

Fig. 8 – (A) Dehydrogenation and (B) rehydrogenation pressure-composition isotherm (PCI) curves of LNL and LNLX (X = Mg, Ca, Ti) samples at 300 °C.

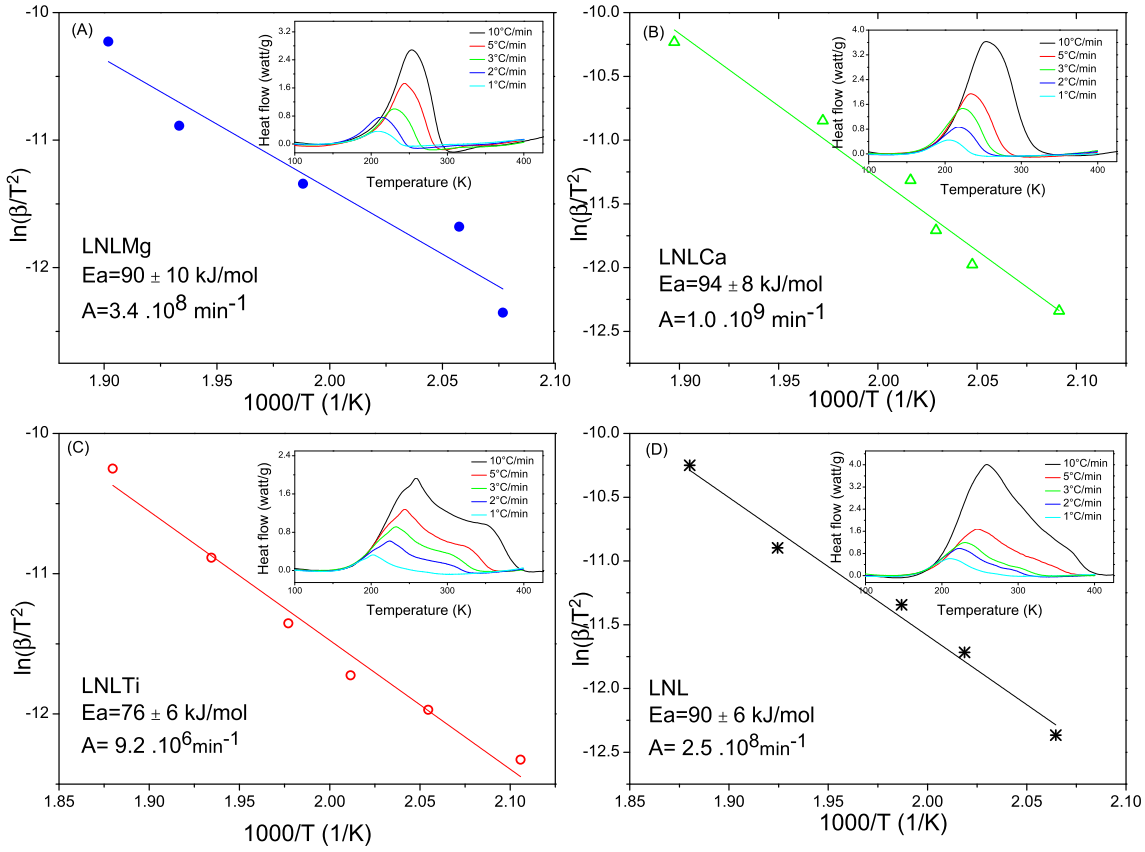

Fig. 9 – Kissinger's plots of the LNL and LNLX samples (X = Mg, Ca, Ti) samples after milling. Inset plots are DSC curves collected at different heating rates (1, 2, 3, 5 and 10 °C/min).

the pristine sample. From DSC curves, the maximum reaction rate temperatures at various heating rates (1, 2, 3, 5 and 10 °C/min) were determined (Fig. 9, inset plots). The Kissinger's plots, *i.e.* the dependency of $\ln(\beta/T_m^{\ 2})$ upon $(1/T_m)$, are displayed in Fig. 9. The dehydrogenation activation energies for LNLMg and LNLCa are *ca.* 90 ± 10 kJ/mol and 94 ± 8 kJ/mol, respectively, which are very similar to that obtained for the unmodified material (90 ± 6 kJ/mol). The E_a for LNLTi sample is 76 ± 6 kJ/mol, which is about 18% reduced from that of the reference material. The values of activation energy look contradictory, because the lower value of activation energy was obtained for LNLTi sample, which presented the worst dehydrogenation kinetics (Figs. 2 and 3). However, the pre-exponential factor of LNLTi is at least 1.5 orders of magnitude reduced respect to unmodified material (see Table 3). To understand the kinetic behavior of the samples, from the calculated values of E_a and A, the specific rate constant *k* at a given temperature is calculated based on the Arrhenius equation ($k = A \exp(-E_a/RT)$). In Table 3 the values of E_a, A and *k* (at 250 and 240 °C) for $LiNH_2$–LiH with and without additives are shown. The values of *k* are consistent with the dehydrogenation rates showed previously (Figs. 2 and 3). The *k* value at 250 °C for LNLMg is 1.2 times greater than that of the unmodified sample, while the *k* value for LNLTi is the lowest. The low A value LNLTi sample could be associated with the fact that TiH_2 prevents the direct contact between $LiNH_2$ and LiH. The presence of crystalline TiH_2 after milling and rehydrogenation is clear (Figs. 4A and 5A), which contrasts with the disappearance of MgH_2 and CaH_2 due to the interaction with $LiNH_2$.

Table 3 – Calculated values of E_a, A and *k* (at 240 and 250 °C).

Sample	E_a (kJ/mol)	A (min^{-1})	*k* at 250 °C (min^{-1})	*k* at 240 °C (min^{-1})
LNLMg	90 ± 10	3.4. 10^8	0.31	0.21
LNLCa	94 ± 8	1.0. 10^9	0.38	0.25
LNLTi	76 ± 6	9.2. 10^6	0.22	0.15
LNL	90 ± 6	2.5. 10^8	0.26	0.17

Isothermal dehydrogenation curves performed at 300 °C for the different composites (Figs. 2A and 3) display an exponential decay behavior in the complete range of hydrogen released as a function of time. Fig. 10A shows the experimental points expressed as conversion α versus time, obtained during the second dehydrogenation cycle for LNLCa and LNL, which ends in about 25 and 40 min, respectively. Similar kinetic behavior was observed after additional hydrogen cycling for all composites. The fitting of these experimental data using an exponential decay function type $\alpha = 1 - e^{-t/\tau}$ is displayed in Fig. 10A. From the fitting it is possible to determine τ as a characteristic parameter of the dehydrogenation rate. Fig. 10B shows the

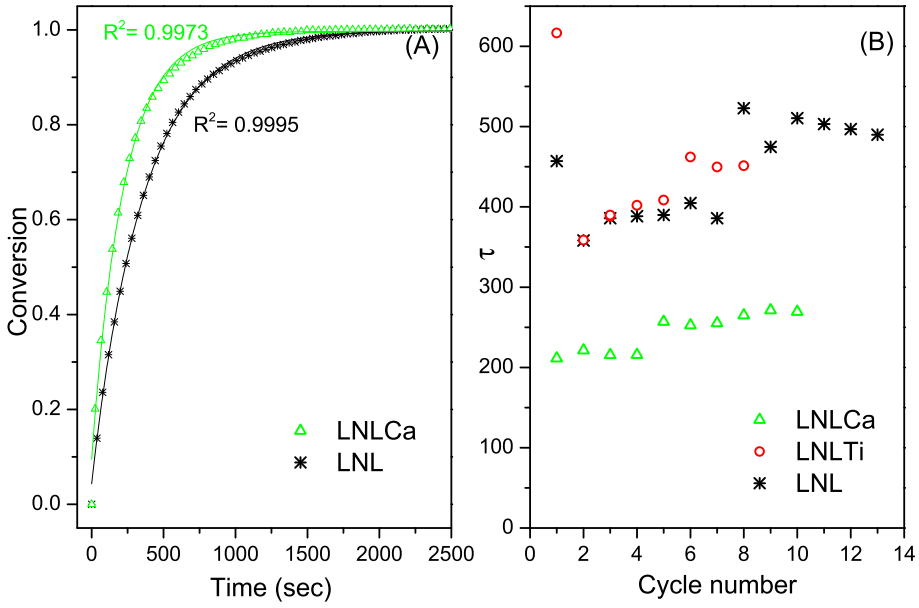

Fig. 10 – A) Conversion versus time for the second dehydrogenation cycle. Symbols: experimental points; continuous line: curve fitting. B) Variation of the characteristic parameter τ as a function of cycle number.

variation of τ during successive hydrogen cycling. Clearly, the characteristic parameter τ represents adequately the different dehydrogenation rates of the $LiNH_2$–LiH system without and with additives (Figs. 2 and 3) and evidences the different times involved to reach the practically complete conversion. The dehydrogenation is characterized by a lower τ for LNLCa composite and this parameter weakly increases with hydrogen cycling. The kinetic mechanism observed is analogous to a first order reaction, where the rate depends on the concentration of one of the reactants and can be interpreted as if the diffusion is the rate-controlling step. Similar kinetic behavior was found for Li–N–H system with the addition of nitride [10]. Hence, dehydrogenation reaction of the composites relies on diffusion control in the complete range of hydrogen release, for unmodified LNL and for LNL with MH_2 added. Recently, David et al. proposed the ion migration model for the hydrogenation/dehydrogenation process of the Li–N–H system [30]. In this model, the principal step is the movement of Li^+ in $LiNH_2$ to create a Frenkel defect pair, charged interstitial $[LiLiNH_2]^+$, and a lithium vacancy $[Li\square NH_2]^-$. Following this idea, Wu et al. proposed that the hydrogen storage of $Li_2Mg(NH)_2$ should also depend strongly on the migration of small mobile ions such as Li^+ and H^+ [21]. Considering these mechanistic understandings, the rate controlling step of dehydrogenation process of the Li–N–H system could be the Li^+ and H^+ mobility within the lithium imide, which could be improved for $LiNH_2$–LiH with MH_2 (M = Mg, Ca) added. Nevertheless, the beneficial effect on the ion mobility for modified composites is not enough to change the controlling step of dehydrogenation. Therefore, to sharply improve the dehydrogenation kinetics of the Li–N–H system with MH_2 added, future investigations should be addressed to increase the diffusion rate of the Li^+ and/or to minimize the diffusion distances.

Conclusions

The $LiNH_2$-1.6LiH with MH_2 added (M = Mg, Ca, Ti) composites were investigated systematically in the present work. Dehydrogenation behavior shows that CaH_2 and MgH_2 are the best additives under the experimental conditions studied, without positive effect of TiH_2. Dehydrogenation rate of LNLCa composite at 300 °C is at least three times faster than unmodified $LiNH_2$-1.6LiH, with about 3.8 wt% of hydrogen reversibly stored. For the Li–Ca–N–H system, the hydrogen storage reversibility involves the formation of 2CaNH–$Ca(NH_2)_2$ solid solution in the hydrogenated state and the Li_2NH–CaNH mixture in the dehydrogenated state. Moreover, MgH_2 reacts with $LiNH_2$ during heating to form $Li_2Mg(NH)_2$, which is not rehydrogenated under the experimental conditions used. A clear thermodynamic destabilization was only observed for $LiNH_2$-1.6LiH with MgH_2 added, with minor effect in the case of CaH_2. Kinetic studies demonstrate that dehydrogenation of $LiNH_2$-1.6LiH system with and without additives is a diffusion controlled reaction. The improvement in the dehydrogenation rates observed for the MgH_2 and CaH_2 addition may be associated with an increment in the mobility of the Li^+ species.

Acknowledgment

This study has been partially supported by CONICET (National Council of Scientific and Technological Research), CNEA (National Commission of Atomic Energy), ANPCyT (PICT N° 1052) and Instituto Balseiro (University of Cuyo). The authors thank to F. Castro for TG measurements. We would also like to thank the Department of Characterization of Materials for the XRD device.

REFERENCES

[1] Walker G. Solid-state hydrogen storage: materials and chemistry. England: Woodhead Publishing Limited; 2008.
[2] Varin R, Czujko T, Wronski Z. Nanomaterials for solid state hydrogen storage. New York: Springer; 2009.
[3] Vajo JJ, Skeith SL, Mertens F. Reversible storage of hydrogen in destabilized $LiBH_4$. J Phys Chem B 2005;109:3719–22.
[4] Böesenberg U, Kim JW, Gosslar D, Eigen N, Jensen TR, Bellosta von Colbe J, et al. Role of additives in $LiBH_4$-MgH_2 reactive hydride composites for sorption kinetics. Acta Mater 2010;58:3381–9.
[5] Gennari FC. Destabilization of $LiBH_4$ by MH_2 (M = Ce, La) for hydrogen storage: nanostructural effects on the hydrogen sorption kinetics. Int J Hydrogen Energy 2011;36:15231–8.
[6] Gennari FC, Fernández Albanesi L, Puszkiel JA, Arneodo Larochette P. Reversible hydrogen storage from $6LiBH_4$-MCl_3 (M= Ce, Gd) composites by in-situ formation of MgH_2. Int J Hydrogen Energy 2011;36:563–70.
[7] Chen P, Xiong Z, Luo J, Lin J, Tan LT. Interaction of hydrogen with metal nitrides and imides. Nature 2002;420:302–4.
[8] Xiong Z, Wu G, Hu J, Chen P. Ternary imides for hydrogen storage. Adv Mater 2004;16:1522–5.
[9] Shaw LL, Osborn W, Markmaitree T, Wan X. The reaction pathway and rate-limiting step of dehydrogenation of the $LiNH_2$ + LiH mixture. J Power Sources 2008;177:500–5.
[10] Nayebossadri S, Aguey-Zinsou KF, Xiao Guo Z. Effect of nitride additives on Li-N-H hydrogen storage system. Int J Hydrogen Energy 2011;36:7920–6.
[11] Fernández Albanesi L, Arneodo Larochette P, Gennari FC. Effect of β-Li_3N phase, Li_2O addition and thermal treatment on the hydrogen sorption behavior of Li_3N. J Power Sources 2012;197:210–7.
[12] Luo WJ. $LiNH_2$-MgH_2: a viable hydrogen storage system. J Alloys Compd 2004;381:284–7.
[13] Luo W, Sickafoose S. Thermodynamic and structural characterization of the Mg–Li–N–H system. J Alloys Compd 2006;407:274–81.
[14] Janot R, Eymery JB, Tarascon JM. Investigation of the processes for reversible hydrogen storage in the Li–Mg–N–H system. J Power Sources 2007;164:496–502.
[15] Rijssenbeek J, Gao Y, Hanson J, Huang Q, Jones C, Toby B. Crystal structure determination and reaction pathway of amide–hydride mixtures. J Alloys Compd 2008;454:233–44.
[16] Kojima Y, Matsumoto M, Kawai Y, Haga T, Ohba N, Miwa K, et al. Hydrogen absorption and desorption by the Li-Al-N-H system. J Phys Chem B 2006;110:9632–6.
[17] Xiong Z, Wu G, Hu J, Liu Y, Chen P, Luo W, et al. Reversible hydrogen storage by a Li-Al-N-H complex. Adv Funct Mater 2007;17:1137–42.
[18] Fernández Albanesi L, Arneodo Lorochette P, Gennari FC. Destabilization of the $LiNH_2$–LiH hydrogen storage system by aluminum incorporation. Int J Hydrogen Energy 2013;38:12325–34.
[19] Hino S, Ichikawa T, Leng H, Fujii H. Hydrogen desorption properties of the Ca–N–H system. J Alloys Compd 2005;398:62–6.
[20] Tokoyoda K, Hino S, Ichikawa T, Okamotoa K, Fujii H. Hydrogen desorption/absorption properties of Li–Ca–N–H system. J Alloys Compd 2007;439:337–41.
[21] Wu H. Structure of ternary imide $Li_2Ca(NH)_2$ and hydrogen storage mechanisms in amide-hydride system. J Am Chem Soc 2008;130:6515–22.
[22] Chu H, Xiong Z, Wu G, He T, Wu C, Chen P. Hydrogen storage properties of Li–Ca–N–H system with different molar ratios of $LiNH_2$/CaH_2. Int J Hydrogen Energy 2010;35:8317–21.
[23] Ichikawa T, Hanada N, Isobe S, Leng HY, Fujii H. Hydrogen storage properties in Ti catalyzed Li–N–H system. J Alloys Compd 2005;404–406:435–8.
[24] Isobe S, Ichikawa T, Hanada N, Leng HY, Fichtner M, Fuhr O, et al. Effect of Ti catalyst with different chemical form on Li–N–H hydrogen storage properties. J Alloys Compd 2005;404–406:439–42.
[25] Matsumoto M, Haga T, Kawai Y, Kojima Y. Hydrogen desorption reactions of Li–N–H hydrogen storage system: estimation of activation free energy. J. Alloys Compd 2007;439:358–62.
[26] Isobe S, Hino S, Ichikawa T, Kojima Y. Identifying catalyst in Li-N-H system by x-ray absorption spectroscopy. Appl Phys Lett 2011;99:13101–3.
[27] Alapati SV, Jonson JK, Sholl DS. Using first principles calculations to identify new destabilized metal hydride reactions for reversible hydrogen storage. Phys Chem Chem Phys 2007;9:1438–52.
[28] Xiong Z, Wu G, Hu J, Chen P. Ca–Na–N–H system for reversible hydrogen storage. J Alloys Compd 2007;441:152–6.
[29] Liang C, Gao MX, Pan HG, Liu YF. Structural transitions of ternary imide $Li_2Mg(NH)_2$ for hydrogen storage. Appl. Phys. Let 2014;105:083909.
[30] David WIF, Jones MO, Gregory DH, Jewell CM, Johnson SR, Walton A. A mechanism for non-stoichiometry in the lithium amide/lithium imide hydrogen storage reaction. J Am Chem Soc 2007;129:1594–601.
[31] Makepeace JW, Jones MO, Callear SK, Edwards PPP, David WDIF. In situ X-ray powder diffraction studies of hydrogen storage and release in the Li–N–H system. Phys Chem Chem Phys 2014;16:4061–70.